

Geometric Optimization of Quantum Control with Minimum Cost

Chengming Tan,¹ Yuhao Cai,² Jinyi Zhang,¹ Shengli Ma,^{2,*} Chenwei Lv,^{3,†} and Ren Zhang^{2,4,‡}

¹Hefei National Research Center for Physical Sciences at the Microscale and School of Physical Sciences, University of Science and Technology of China, Hefei 230026, China

²MOE Key Laboratory for Nonequilibrium Synthesis and Modulation of Condensed Matter, Shaanxi Province Key Laboratory of Quantum Information and Quantum Optoelectronic Devices, School of Physics, Xi'an Jiaotong University, Xi'an 710049, China

³Department of Physics, Oklahoma University, Norman, Oklahoma 73072, USA

⁴Hefei National Laboratory, Hefei, 230088, China

(Dated: September 24, 2024)

We study the optimization of quantum control from the perspective of differential geometry. Here, optimal quantum control takes the minimum cost of transporting a quantum state. By defining a cost function, we quantify the cost by the length of a trajectory in the relevant Riemannian manifold. We demonstrate the optimization protocol using SU(2) and SU(1,1) dynamically symmetric systems, which cover a large class of physical scenarios. For these systems, time evolution is visualized in the three-dimensional manifold. Given the initial and final states, the minimum-cost quantum control corresponds to the geodesic of the manifold. When the trajectory linking the initial and final states is specified, the minimum-cost quantum control corresponds to the geodesic in a sub-manifold embedded in the three-dimensional manifold. Optimal quantum control in this situation provides a geometrical means of optimizing shortcuts to adiabatic driving.

Introduction. Geometry is the cornerstone that unifies different realms of physics. An example is the fibre bundle, a central concept of differential geometry that serves as the mathematical foundation for gauge theory and general relativity. By geometrizing the notion in physics, we can obtain a deeper and more comprehensive understanding of many longstanding problems. It has been demonstrated that questions of the minimum time for state transferring [1–14], the optimal designation of the quantum circuit [15–17], and a speed limit to quantum information processing [18–27] can be mapped to the question of finding the geodesic on Riemannian manifolds. The geometrization paradigm also providing a quantitative measure of complexity in a plethora of systems [16, 17, 28–32].

One of the major goals of optimal quantum controls is the pursuit of reliable operations with the utmost efficiency, such achieving quantum speed limit and high fidelity [33–37]. Traditionally, the constraint on energy cost is not widely imposed, presupposing an inexhaustible supply of energy during the operation. However, recent studies have shown that even for a single particle, the trade-off between speed and cost is substantial [38–41]. Moreover, the realization of noise-resistant quantum computation necessitates highly scalable systems, such as neutral atoms entrapped in tweezers, superconducting circuits, and trapped ions [42–59]. Most of the operations are facilitated by laser or electromagnetic fields, the power of which is inherently finite. Therefore, it is highly desirable to identify an optimal quantum control approach that minimizes cost.

Inspired by previous studies on the geometrization, this work presents a quantum control strategy that minimizes the cost during the operation. We formulate the problem as identifying the geodesics within a Riemannian manifold or its sub-manifold.

Our main conclusions are summarized as follows: (1) Given the initial and final states, we provide an optimal trajectory to drive the system from the initial state to the final state. (2) When the initial and final states, as well as the desired evolution path, are specified, we offer a time-dependent Hamiltonian that facilitates this precise evolution and optimizes it with minimal cost. (3) We demonstrate the applicability of our method in systems with SU(2) or SU(1,1) dynamical symmetry, which covers a large class of physical settings [60–76].

SU(2) dynamical system. We start with the SU(2) dynamically symmetric system, which is ubiquitous across multidisciplinary physics. The dynamically symmetric system refers to the system whose Hamiltonian can be written as certain symmetry group generators. Without loss of generality, we consider a spin-1/2 subject to a time-dependent magnetic field $\mathbf{B}(t) = (B_x(t), B_y(t), B_z(t))$. The Pauli matrices $\hat{\sigma}_{x,y,z}$ couple to the magnetic field and serve as the two-dimensional representation of the $\mathfrak{su}(2)$ algebra. Generally, the state can be represented by a point on a two-dimensional manifold, i.e., the Bloch sphere, and the wavefunction is written as $|\varphi(\theta, \phi)\rangle = (-e^{-i\phi/2} \sin(\theta/2), e^{i\phi/2} \cos(\theta/2))^T$, where θ, ϕ denote the spherical coordinates on the Bloch sphere. It is allowed to attach a global phase factor $e^{i\eta}$ to the wavefunction. We will show that η plays a significant role in the minimum-cost quantum control. The time evolution of the system can be viewed as a trajectory in the parameter space spanned by θ, ϕ , and η , which are time-dependent. We will omit the argument t for brevity.

To measure the cost associated with a particular trajectory, we construct a parameterization of the propagator $\hat{U} = \exp(-i\frac{\phi}{2}\hat{\sigma}_z) \exp(-i\frac{\theta}{2}\hat{\sigma}_y) \exp(-i\eta\hat{\sigma}_z)$. It can

be verified that $e^{i\eta}|\varphi(\theta, \phi)\rangle = \hat{U}(\theta, \phi, \eta)|\varphi(0, 0)\rangle$, which means that the trajectory of the system is equivalent to that of the propagator. With the propagator, we can design various magnetic field configurations driving the system from the initial to the final state along various trajectories ϕ, θ, η . The question arises: Which one has the minimum cost? To address this question, we first define the time-dependent Hamiltonian through the propagator,

$$\hat{H}(t) = i(\partial_t \hat{U}(t))\hat{U}^{-1}(t) = - \sum_{i=x,y,z} B_i(t)\hat{\sigma}_i, \quad (1)$$

where we set the Bohr magnetic moment and Planck's constant $\mu_B = 1$, $\hbar = 1$. The time-dependent magnetic field is derived from $B_i(t) = \text{Tr}[\hat{H}(t)\sigma_i^\dagger]/2$. The explicit expressions are given by $B_x(t) = (\partial_t \eta) \cos \phi \sin \theta - (\partial_t \theta)/2 \sin \phi$, $B_y(t) = (\partial_t \eta) \sin \phi \sin \theta + (\partial_t \theta)/2 \cos \phi$, $B_z(t) = (\partial_t \eta) \cos \theta + (\partial_t \phi)/2$.

Next, we define the cost through the cost function

$$ds^2 = \sum_{i=x,y,z} \mathcal{I}_i^2 B_i^2 dt^2, \quad (2)$$

where the dimensionless coefficient \mathcal{I}_i represents the difficulty to apply the external field along i -th direction. In our case, we consider the isotropic cost that $\mathcal{I}_i = 1/2$. The total cost of evolution is the integral of the cost function from the initial state to the final state $s = \int_{s_i}^{s_f} ds = \frac{1}{2} \int_{t_i}^{t_f} |\mathbf{B}(t)| dt$. Upon substituting the explicit expression of $B_i(t)$'s into Eq. (2), the cost function is recast as the line element in the parameter space,

$$ds^2 = (d\eta + \cos \theta d\phi/2)^2 + (d\theta^2 + \sin^2 \theta d\phi^2)/4, \quad (3)$$

making the parameter manifold into a Riemannian manifold as a three-sphere. Therefore, the problem of optimizing the evolution with the minimum cost is transformed into finding the trajectory with the shortest length in the parameter space equipped with the metric Eq. 3. Since η is the global phase, the wavefunctions with different η describe the same state. By imposing $2d\eta = \cos \theta d\phi$, we minimize the cost, showing the importance of η in the minimum-cost control. Now, we consider two different scenarios.

(I). Starting with an initial state, we now show the minimum cost to achieve the desired target state. We first consider that their phases are also fixed. Geometrically, this means identifying the geodesic which links two points in the manifold spanned by θ, ϕ and η , the metric of which is given in Eq.(3). To this end, we must solve its geodesic equation

$$\begin{aligned} \partial_t^2 \eta &= -\cot \theta \partial_t \eta \partial_t \theta + \csc \theta (\partial_t \phi \partial_t \theta)/2; \\ \partial_t^2 \theta &= -2 \sin \theta (\partial_t \eta \partial_t \phi); \\ \partial_t^2 \phi &= 2 \csc \theta (\partial_t \eta \partial_t \theta) - \cot \theta (\partial_t \phi \partial_t \theta). \end{aligned} \quad (4)$$

The initial point $(\theta_i, \phi_i, \eta_i)$ and target point $(\theta_f, \phi_f, \eta_f)$ serve as the boundary conditions. By solving the Eq.(4),

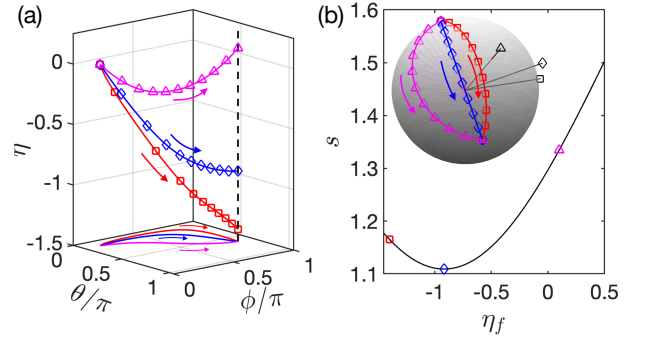


FIG. 1. The evolution trajectory from the initial $(\theta_i, \phi_i, 0)$ to the final state $(\theta_f, \phi_f, \eta_f)$ for SU(2) symmetric system. The markers distinguish different final global phase η_f . (a) The colored lines with markers are the geodesic on space (θ, ϕ, η) . The colored lines without markers are the projection on the reduced (θ, ϕ) space. The blue line with diamonds is the trajectory of which the projection on reduced space is also the geodesic. Other parameters are chosen as $\theta_i = \pi/8, \theta_f = 5\pi/8, \phi_i = \pi/8$ and $\phi_f = 7\pi/8$. (b) The length of the geodesics with different η_f . Inset: The projection of trajectories (colored lines with markers) on the Bloch sphere and the direction of driving fields (black markers).

we determine the geodesic that links the initial and target points, which is represented by the parametric functions $(\theta(t), \phi(t), \eta(t))$. Physically, we obtain an instantaneous magnetic field $(B_x(t), B_y(t), B_z(t))$ that minimizes the cost. In Fig. 1(a), we depict the geodesics between different points, as shown by colored lines with markers. The parameters are chosen as $\theta_i = \pi/8, \theta_f = 5\pi/8, \phi_i = \pi/8, \phi_f = 7\pi/8, \eta_i = 0$, and η_f varies.

Considering the different η_f 's correspond to the same state, we may further reduce the cost by selecting an optimal η_f . Geometrically, we need to identify the shortest geodesic from the starting point $(\theta_i, \phi_i, 0)$ to the fibre (black dashed line in Fig. 1a) sitting on (θ_f, ϕ_f) . Referring to Eq. (3), the first term should vanish, and the optimal phase at time t is

$$\eta_{\text{opt}}(t) = -\frac{1}{2} \int_{t_i}^t \cos \theta(\tau) [\partial_\tau \phi(\tau)] d\tau. \quad (5)$$

The reduced metric reads $ds^2 = \frac{1}{4}(d\theta^2 + \sin^2 \theta d\phi^2)$, which is the metric of a two-sphere with radius $1/2$. The geodesic equation set then reduces to

$$\begin{aligned} \partial_t^2 \theta &= \sin \theta \cos \theta (\partial_t \phi)^2; \\ \partial_t^2 \phi &= -2 \cot \theta (\partial_t \phi \partial_t \theta). \end{aligned} \quad (6)$$

Subject to the boundary conditions (θ_i, ϕ_i) and (θ_f, ϕ_f) , we solve the geodesic equation set in Eq.(6). The resulting geodesic, represented by the parametric functions $(\theta(t), \phi(t))$, traces the minor arc on the Bloch sphere. It is verified that $(\theta(t), \phi(t), \eta(t))$ is the shortest geodesic linking $(\theta_i, \phi_i, 0)$ to the fibre on (θ_f, ϕ_f) within the three-dimensional manifold. Guided by the geodesic, we can

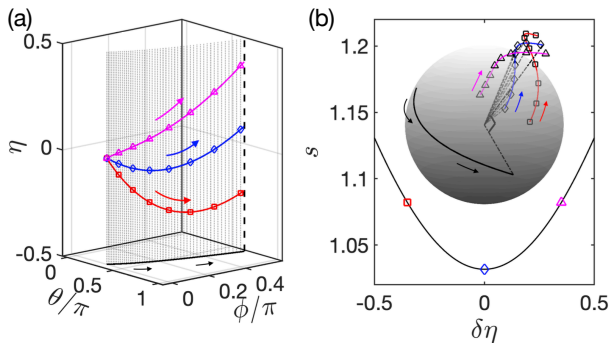


FIG. 2. The evolution along $(\theta(t), \phi(t))$ for $SU(2)$ symmetric system. The markers distinguish deviation $\delta\eta$ to $\eta_{\text{opt}}(t)$ in Eq.(5). (a) The colored lines with markers all satisfy the constraint of $\theta(t)$ and $\phi(t)$, represented by the black solid line. The blue line with diamonds is the trajectory with minimum cost. (b) The length of the trajectory with different $\delta\eta$. Inset: The projection of trajectories (black line without marker) and the direction of driving fields (black markers).

construct a Hamiltonian with the instantaneous magnetic field that leads to the minimum cost.

In Fig.1(a), we depict geodesics in the three-dimensional manifold and their projections on the reduced two-dimensional manifold with varying η_f . The shortest one is represented by the blue line with diamonds, and its projection remains a geodesic on the reduced two-dimensional manifold. This property is not shared by the non-shortest geodesics, marked by red rectangles and pink triangles. Fig. 1(b) shows the geodesic lengths for different final global phases η_f , clearly showing an increase in the geodesic length as η_f deviates from the optimal value. The state trajectories can be visualized on the Bloch sphere, as shown in the inset of Fig. 1(b). The magnetic field directions are indicated by black markers matching the shape of the state trajectories. For minimum-cost driving, the state trajectory is a minor arc of the Bloch sphere, with the magnetic field perpendicular to the plane containing the arc and the radius. It is worth mentioning that the Hamiltonian in the minimal-cost driving protocol of $SU(2)$ considered here is time-independent, and the geometric phase alone contributes to the accumulated phase. Other driving methods do not share this property.

(II). In addition to the initial (θ_i, ϕ_i) and target (θ_f, ϕ_f) states on the Bloch sphere, we also fix the trajectory between them, specified as $(\theta(t), \phi(t))$ for $t \in [0, t_f]$ where the initial time $t_i = 0$. To drive the system along the given trajectory, one strategy is adiabatic driving with a magnetic field aligned with $(\theta(t), \phi(t))$. In the adiabatic limit, this results in an infinitely large dynamical phase and cost. An alternative is the shortcut to adiabatic driving (STAD), which accelerates the state transportation and suppresses the excitation [38, 77–82]. A key question is: Is there an optimal STAD that minimizes the cost?

Similar to **(I)**, η offers the flexibility to minimize the cost defined in Eq.(3). We use an example to demonstrate the process. The solid black line in Fig. 2(a) traces a particular trajectory of the state,

$$\theta(t) = \pi/3 + \pi t/(3t_f); \phi(t) = \pi t^2/(3t_f^2) + \pi t/(4t_f). \quad (7)$$

By attaching a fibre on each point on the trajectory, we construct a sub-manifold defined by (t, η) (denoted by the black dots) embedded in the parameter space. Any trajectory in the sub-manifold that links $(\theta_i, \phi_i, 0)$ to the fibre on (θ_f, ϕ_f) represents a STAD, as indicated by colored lines with markers. Substituting Eq. (7) into Eq. (5) yields the shortest trajectory, denoted by the blue line with diamonds in Fig. 2(a). We have confirmed that the cost increases when we deviate from this trajectory, through the addition of $\delta\eta \sin\left(\frac{\pi t}{3t_f}\right)$ to $\eta(t)$, as shown by the rectangle and triangle in Fig. 2(b). The corresponding trajectories are displayed in Fig. 2(a). For each trajectory on the sub-manifold, the instantaneous magnetic field is obtained, as shown by the color lines with markers in the inset of Fig. 2(b). We find that for the minimum-cost STAD, the instantaneous vector field $\mathbf{B}(t)$ is always perpendicular to the current state trajectory (black curve on the Bloch sphere). Again, this condition may not hold universally for other scenarios.

We would like to point out a profound geometric root for the minimum-cost STAD. Substituting Eq.(7) into Eq.(3) leads to the induced metric of the sub-manifold. The shortest geodesic linking $(t = 0, \eta = 0)$ and the line $t = t_f$ could be obtained by solving the geodesic equation on the sub-manifold. We verified that the blue line in Fig. 2(a) that minimizes the cost is indeed the shortest geodesic on the sub-manifold.

SU(1,1) dynamical system. We now consider the systems with $SU(1,1)$ dynamical symmetry. The generators of $SU(1,1)$ group obey the commutation relations $[\hat{K}_0, \hat{K}_1] = i\hat{K}_2, [\hat{K}_1, \hat{K}_2] = -i\hat{K}_0, [\hat{K}_2, \hat{K}_0] = i\hat{K}_1$. The representation of the $\mathfrak{su}(1,1)$ algebra is prevalent across various disciplines, including the harmonic and anharmonic oscillators, single- and two-mode squeezing operations, and spin-1/2 particles in complex magnetic fields, among others [31, 61–69].

In analogy to the $SU(2)$ case, the state $|\psi(\rho, \phi)\rangle$ can be represented by a point on a two-dimensional manifold parameterized by ρ and ϕ . To quantify the cost of driving $|\psi(0, 0)\rangle$ to $|\psi(\rho, \phi)\rangle$, we define a propagator $\hat{U} = \exp\left(-i\frac{\phi}{2}\hat{K}_0\right)\exp\left(-i\frac{\rho}{2}\hat{K}_2\right)\exp\left(-i\eta\hat{K}_0\right)$, where $\rho \in [0, +\infty)$. As such, $e^{i\eta}|\psi(\rho, \phi)\rangle = \hat{U}|\psi(0, 0)\rangle$. The evolution of the $SU(1,1)$ dynamically symmetric system traces a trajectory in the parameter space (ρ, ϕ, η) , which is generated by the time-dependent Hamiltonian $\hat{H}(t) = i(\partial_t \hat{U}(t))\hat{U}^{-1}(t) = \sum_i \xi_i(t)\hat{K}_i$. The field strength in the i -th direction is derived from the Hamiltonian: $\xi_i(t) = \text{Tr}[\hat{H}(t)\hat{K}_i^\dagger]/2$. Explicitly, we have $\xi_0(t) = (\partial_t \eta) \cosh \rho +$

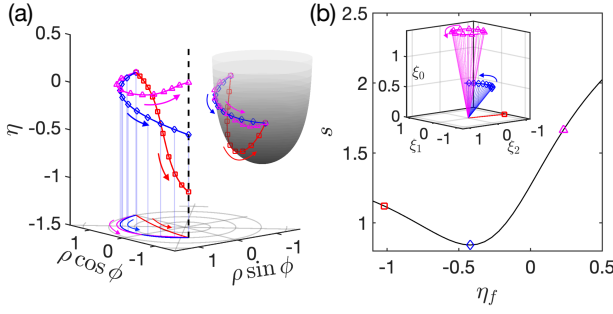


FIG. 3. The evolution trajectory from the initial $(\rho_i, \phi_i, 0)$ to the final state (ρ_f, ϕ_f, η_f) for SU(1,1) symmetric system. The markers distinguish different final phase η_f . (a) The colored lines with markers are the geodesic on space (ρ, ϕ, η) . The colored lines without markers are the projection on the reduced (ρ, ϕ) space. The blue line with diamonds is the trajectory of which the projection on reduced space is also the geodesic. Other parameters are $\rho_i = 1.5, \phi_i = 0, \rho_f = 1.0$ and $\phi_f = 4\pi/5$. Inset: The curved surface of reduced space embedded in a flat 3-dimensional Euclidean space. (b) The length of the geodesics as a function of η_f . Inset: The driving field (colored lines with markers).

$(\partial_t \phi)/2, \xi_1(t) = (\partial_t \eta) \cos \phi \sinh \rho - (\partial_t \rho)/2 \sin \phi, \xi_2(t) = (\partial_t \eta) \sin \phi \sinh \rho + (\partial_t \rho)/2 \cos \phi$. The cost function is then defined as $ds^2 = \frac{1}{4}(\xi_0^2 + \xi_1^2 + \xi_2^2)dt^2$. Inserting the explicit expression of $\xi_i(t)$ into the cost function yields the metric of the parameter space,

$$ds^2 = \left(\sqrt{\cosh 2\rho} d\eta + \cosh \rho / \left(2\sqrt{\cosh 2\rho} \right) d\phi \right)^2 + (d\rho^2 + \sinh^2 \rho / \cosh(2\rho) d\phi^2) / 4. \quad (8)$$

With this metric, optimal quantum control for the SU(1,1) dynamical system can be engineered by employing a method analogous to the SU(2) case. By setting $d\eta = -\cosh \rho / (2\cosh 2\rho) d\phi$, we can achieve the minimum-cost driving. Now, we explore two scenarios.

(I). Given the initial state $(\rho_i, \phi_i, 0)$ and final state (ρ_f, ϕ_f, η_f) , we solve the geodesic equations of the parameter space with metric Eq. (8), which are written as

$$\begin{aligned} \partial_t^2 \eta &= -3 \coth \rho (\partial_t \eta \partial_t \rho) - \operatorname{csch} \rho (\partial_t \rho \partial_t \phi) / 2; \\ \partial_t^2 \rho &= 4 \sinh(2\rho) (\partial_t \eta)^2 + 2 \sinh \rho (\partial_t \eta \partial_t \phi); \\ \partial_t^2 \phi &= \frac{4 + 2 \cosh(2\rho)}{\sinh \rho} (\partial_t \eta \partial_t \rho) + \coth \rho (\partial_t \rho \partial_t \phi). \end{aligned} \quad (9)$$

In Fig. 3(a), the colored lines with markers are the geodesics. Each line corresponds to the minimum cost driving the system from the initial state $|\psi(\rho_i, \phi_i)\rangle$ to the respective final state $e^{i\eta_f} |\psi(\rho_f, \phi_f)\rangle$, with different η_f 's.

Considering different η_f 's correspond to the same state, we further reduce the cost by selecting the optimal η_f . To achieve this, we seek the shortest geodesic from the starting point to the fibre attached to the target point (ρ_f, ϕ_f) (dash black line). According to Eq.(8), the opti-

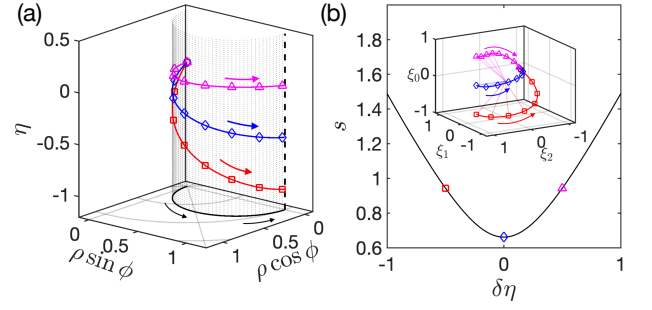


FIG. 4. The evolution along $(\rho(t), \phi(t))$ for SU(1,1) symmetric system. The markers distinguish different deviation $\delta\eta$ to $\eta_{\text{opt}}(t)$. (a) The colored lines with markers all satisfy the constraint of $\rho(t)$ and $\phi(t)$, which is represented by the black solid line. The blue line with diamonds is the trajectory with minimum cost. (b) The trajectory length as a function of $\delta\eta$. Inset: The corresponding driving field.

mal $\eta_{\text{opt}}(t)$ reads

$$\eta_{\text{opt}}(t) = - \int_{t_i}^t \frac{\cosh \rho(\tau)}{2 \cosh 2\rho(\tau)} [\partial_\tau \phi(\tau)] d\tau, \quad (10)$$

and the reduced metric is $ds^2 = (d\rho^2 + \sinh^2 \rho / \cosh 2\rho d\phi^2) / 4$. The integrand in Eq.(10) is derived by solving the reduced geodesic equation set,

$$\begin{aligned} \partial_t^2 \rho &= \operatorname{sech}(2\rho) \tanh(2\rho) (\partial_t \phi)^2 / 2; \\ \partial_t^2 \phi &= -2 \coth \rho \operatorname{sech}(2\rho) \partial_t \rho \partial_t \phi. \end{aligned} \quad (11)$$

With the boundary conditions (ρ_i, ϕ_i) and (ρ_f, ϕ_f) , we solve Eq.(11) and substitute the solution to Eq.(10). This yields the shortest geodesic $(\rho(t), \phi(t), \eta_{\text{opt}}(t))$ with $t \in [t_i, t_f]$, as shown by the blue line with diamond in Fig. 3(a), and its projection (blue line) in the ρ - ϕ plane is the solution of Eq.(11). The length of geodesics for different final phases η_f are depicted in Fig. 3(b), demonstrating that the results of Eq.(11) and (10) indeed take the minimum cost, with deviations costing more. The driving field $(\xi_0(t), \xi_1(t), \xi_2(t))$ is demonstrated in the inset of Fig. 3(b).

By embedding the reduced manifold in the three-dimensional flat Euclidean space, we visualize the state evolution on a two-dimensional curved space, as depicted in the inset of Fig. 3(a). This serves as the SU(1,1) counterpart to the Bloch sphere in the SU(2) system. The projection of the geodesic (with diamond) onto the two-dimensional curved space is again a geodesic, as illustrated in the inset of Fig. 3(a).

(II). Similar to the SU(2) case, we can also specify the trajectory of the state evolution. For illustration, we consider the following trajectory for $t \in [0, t_f]$,

$$\rho(t) = \sin(\pi t / (2t_f)); \phi(t) = \pi t / (2t_f), \quad (12)$$

as shown by the black solid line in Fig. 4(a). By attaching a fibre at each point along this trajectory, we obtain the embedded surface, represented by the black dots.

Substituting Eq.(12) into Eq.(10), the optimal $\eta_{\text{opt}}(t)$ is determined. In conjunction with $(\rho(t), \phi(t))$, this yields the shortest trajectory (blue diamond line) on the embedded surface. The corresponding optimal driving field can also be derived. It is important to note that this field can alternatively be obtained by solving the geodesic equation on the embedded surface. To show that the cost is minimized by the optimal $\eta_{\text{opt}}(t)$, we introduce a slight deviation from the optimal phase as $\eta(t) = \delta\eta \sin\left(\frac{\pi t}{2t_f}\right) + \eta_{\text{opt}}(t)$. The lengths of trajectories for various $\delta\eta$ are depicted in Fig.4(b), where $\delta\eta = 0$ corresponds to the shortest length (diamond). Non-zero deviations lengthen the trajectory, thereby increase the cost. The respective driving field $(\xi_0(t), \xi_1(t), \xi_2(t))$ for this scenario is displayed in the inset of Fig. 4(b), exhibiting both time-varying strength and direction.

Conclusion-. We have investigated the optimization of quantum control in dynamical symmetric systems using differential geometry. The optimal quantum control taking the minimum cost corresponds to the shortest geodesic on a differential manifold. We utilized the SU(2) and SU(1,1) dynamical symmetric systems to illustrate the optimization process. When only the initial and final states are specified, the minimum-cost trajectory corresponds to the shortest geodesic on the three-dimensional manifold; when a trajectory between these states is also prescribed, the minimum-cost trajectory lies on an embedded two-dimensional sub-manifold, which is optimal for STAD. Addressing cost issues is crucial for scalable quantum computation, such as in atomic arrays, making our findings applicable to specific systems. Our approach can be generalized to systems with higher symmetries, such as two-spin quantum control. Moreover, considering anisotropic costs, as shown in Eq. (2), warrants further investigation for a broader class of quantum systems.

We are grateful to Qi Zhou, Peng Zhang, Xiaoling Cui and Liang Mao for helpful discussions. This work is supported by the Innovation Program for Quantum Science and Technology (Grants No.2021ZD0302001), NSFC (Grants No.12174300 and No.12374248), the Fundamental Research Funds for the Central Universities (Grant No. 71211819000001) and Tang Scholar.

* msl1987@xjtu.edu.cn

† lcw205046@gmail.com

‡ renzhang@xjtu.edu.cn

- [1] N. Khaneja, R. Brockett, and S. J. Glaser, Time optimal control in spin systems, *Phys. Rev. A* **63**, 032308 (2001).
- [2] A. Carlini, A. Hosoya, T. Koike, and Y. Okudaira, Time-optimal quantum evolution, *Phys. Rev. Lett.* **96**, 060503 (2006).
- [3] A. Carlini, A. Hosoya, T. Koike, and Y. Okudaira, Time-optimal unitary operations, *Phys. Rev. A* **75**, 042308 (2007).
- [4] A. Carlini, A. Hosoya, T. Koike, and Y. Okudaira, Time optimal quantum evolution of mixed states, *Journal of Physics A: Mathematical and Theoretical* **41**, 045303 (2008).
- [5] G. C. Hegerfeldt, Driving at the quantum speed limit: Optimal control of a two-level system, *Phys. Rev. Lett.* **111**, 260501 (2013).
- [6] X. Wang, M. Allegra, K. Jacobs, S. Lloyd, C. Lupo, and M. Mohseni, Quantum brachistochrone curves as geodesics: Obtaining accurate minimum-time protocols for the control of quantum systems, *Phys. Rev. Lett.* **114**, 170501 (2015).
- [7] J. Geng, Y. Wu, X. Wang, K. Xu, F. Shi, Y. Xie, X. Rong, and J. Du, Experimental time-optimal universal control of spin qubits in solids, *Phys. Rev. Lett.* **117**, 170501 (2016).
- [8] L. Garcia, J. M. Bofill, I. d. P. R. Moreira, and G. Alameda, Highly adiabatic time-optimal quantum driving at low energy cost, *Phys. Rev. Lett.* **129**, 180402 (2022).
- [9] K. W. Moore Tibbetts, C. Brif, M. D. Grace, A. Donovan, D. L. Hocker, T.-S. Ho, R.-B. Wu, and H. Rabitz, Exploring the tradeoff between fidelity and time optimal control of quantum unitary transformations, *Phys. Rev. A* **86**, 062309 (2012).
- [10] M. A. Nielsen, M. R. Dowling, M. Gu, and A. C. Doherty, Optimal control, geometry, and quantum computing, *Phys. Rev. A* **73**, 062323 (2006).
- [11] G. C. Hegerfeldt, Driving at the quantum speed limit: Optimal control of a two-level system, *Phys. Rev. Lett.* **111**, 260501 (2013).
- [12] R. Romano, Geometric analysis of minimum-time trajectories for a two-level quantum system, *Phys. Rev. A* **90**, 062302 (2014).
- [13] F. Albertini and D. D'Alessandro, Minimum time optimal synthesis for two level quantum systems, *Journal of Mathematical Physics* **56**, 012106 (2015).
- [14] C. Jameson, B. Basyildiz, D. Moore, K. Clark, and Z. Gong, Time optimal quantum state transfer in a fully-connected quantum computer, *Quantum Science and Technology* **9**, 015014 (2023).
- [15] J. Anandan and Y. Aharonov, Geometry of quantum evolution, *Phys. Rev. Lett.* **65**, 1697 (1990).
- [16] M. A. Nielsen, M. R. Dowling, M. Gu, and A. C. Doherty, Quantum computation as geometry, *Science* **311**, 1133 (2006).
- [17] A. R. Brown and L. Susskind, Complexity geometry of a single qubit, *Phys. Rev. D* **100**, 046020 (2019).
- [18] G. N. Fleming, A unitarity bound on the evolution of nonstationary states, *Nuov Cim A* **16**, 232 (1973).
- [19] K. Bhattacharyya, Quantum decay and the mandelstam-tamm-energy inequality, *Journal of Physics A: Mathematical and General* **16**, 2993 (1983).
- [20] N. Margolus and L. B. Levitin, The maximum speed of dynamical evolution, *Physica D: Nonlinear Phenomena* **120**, 188 (1998), proceedings of the Fourth Workshop on Physics and Consumption.
- [21] L. B. Levitin and T. Toffoli, Fundamental limit on the rate of quantum dynamics: The unified bound is tight, *Phys. Rev. Lett.* **103**, 160502 (2009).
- [22] P. J. Jones and P. Kok, Geometric derivation of the quantum speed limit, *Phys. Rev. A* **82**, 022107 (2010).
- [23] M. M. Taddei, B. M. Escher, L. Davidovich, and R. L. de Matos Filho, Quantum speed limit for physical processes, *Phys. Rev. Lett.* **110**, 050402 (2013).

- [24] B. Russell and S. Stepney, Zermelo navigation and a speed limit to quantum information processing, *Phys. Rev. A* **90**, 012303 (2014).
- [25] D. P. Pires, M. Cianciaruso, L. C. Céleri, G. Adesso, and D. O. Soares-Pinto, Generalized geometric quantum speed limits, *Phys. Rev. X* **6**, 021031 (2016).
- [26] M. Bukov, D. Sels, and A. Polkovnikov, Geometric speed limit of accessible many-body state preparation, *Phys. Rev. X* **9**, 011034 (2019).
- [27] G. Ness, A. Alberti, and Y. Sagi, Quantum speed limit for states with a bounded energy spectrum, *Phys. Rev. Lett.* **129**, 140403 (2022).
- [28] M. Zhang, H.-M. Yu, and J. Liu, Quantum speed limit for complex dynamics, *npj Quantum Information* **9** (2023), 10.1038/s41534-023-00768-8.
- [29] C. Lv, R. Zhang, and Q. Zhou, Building krylov complexity from circuit complexity, (2023), arXiv:2303.07343 [quant-ph].
- [30] S. Malikis and V. Cheianov, Integrability and chaos in the quantum brachistochrone problem, *Phys. Rev. A* **110**, 022205 (2024).
- [31] C. Lv and Q. Zhou, Emergent spacetimes from hermitian and non-hermitian quantum dynamics, (2023), arXiv:2205.07429 [cond-mat.quant-gas].
- [32] P. Caputa, J. M. Magan, and D. Patramanis, Geometry of krylov complexity, *Phys. Rev. Res.* **4**, 013041 (2022).
- [33] G. Li, J.-F. Chen, C. P. Sun, and H. Dong, Geodesic path for the minimal energy cost in shortcuts to isothermality, *Phys. Rev. Lett.* **128**, 230603 (2022).
- [34] S. S. Hegde, J. Zhang, and D. Suter, Toward the speed limit of high-fidelity two-qubit gates, *Phys. Rev. Lett.* **128**, 230502 (2022).
- [35] J. Howard, A. Lidiak, C. Jameson, B. Basyildiz, K. Clark, T. Zhao, M. Bal, J. Long, D. P. Pappas, M. Singh, and Z. Gong, Implementing two-qubit gates at the quantum speed limit, *Phys. Rev. Res.* **5**, 043194 (2023).
- [36] X. Cao, J. Cui, M. H. Yung, and R.-B. Wu, Robust control of single-qubit gates at the quantum speed limit, *Phys. Rev. A* **110**, 022603 (2024).
- [37] V. Negîrneac, H. Ali, N. Muthusubramanian, F. Battistel, R. Sagastizabal, M. S. Moreira, J. F. Marques, W. J. Vlothuizen, M. Beekman, C. Zachariadis, N. Haider, A. Bruno, and L. DiCarlo, High-fidelity controlled- z gate with maximal intermediate leakage operating at the speed limit in a superconducting quantum processor, *Phys. Rev. Lett.* **126**, 220502 (2021).
- [38] J.-W. Zhang, J.-T. Bu, J. C. Li, W. Meng, W.-Q. Ding, B. Wang, W.-F. Yuan, H.-J. Du, G.-Y. Ding, W.-J. Chen, L. Chen, F. Zhou, Z. Xu, and M. Feng, Single-atom verification of the optimal trade-off between speed and cost in shortcuts to adiabaticity, *Phys. Rev. Lett.* **132**, 213602 (2024).
- [39] S. Campbell and S. Deffner, Trade-off between speed and cost in shortcuts to adiabaticity, *Phys. Rev. Lett.* **118**, 100601 (2017).
- [40] Y. Zheng, S. Campbell, G. De Chiara, and D. Poletti, Cost of counterdiabatic driving and work output, *Phys. Rev. A* **94**, 042132 (2016).
- [41] K. Z. Li and D. M. Tong, Geometric property of energetic cost in transitionless quantum driving, *Phys. Rev. A* **106**, 052414 (2022).
- [42] M. Saffman, T. G. Walker, and K. Mølmer, Quantum information with rydberg atoms, *Rev. Mod. Phys.* **82**, 2313 (2010).
- [43] D. Barredo, S. de Léséleuc, V. Lienhard, T. Lahaye, and A. Browaeys, An atom-by-atom assembler of defect-free arbitrary two-dimensional atomic arrays, *Science* **354**, 1021 (2016).
- [44] Y. Miroshnychenko, W. Alt, I. Dotsenko, L. Förster, M. Khudaverdyan, D. Meschede, D. Schrader, and A. Rauschenbeutel, An atom-sorting machine. *Nature*. **442**, 151 (2006).
- [45] A. M. Kaufman and K.-K. Ni, Quantum science with optical tweezer arrays of ultracold atoms and molecules. *Nat. Phys.* **17**, 1324–1333 (2021).
- [46] M. Endres, H. Bernien, A. Keesling, H. Levine, E. R. Anschuetz, A. Krajenbrink, C. Senko, V. Vuletic, M. Greiner, and M. D. Lukin, Atom-by-atom assembly of defect-free one-dimensional cold atom arrays, *Science* **354**, 1024 (2016).
- [47] C. Robens, J. Zopes, W. Alt, S. Brakhane, D. Meschede, and A. Alberti, Low-entropy states of neutral atoms in polarization-synthesized optical lattices, *Phys. Rev. Lett.* **118**, 065302 (2017).
- [48] A. Kumar, T.-Y. Wu, F. Giraldo, and D. S. Weiss, Sorting ultracold atoms in a three-dimensional optical lattice in a realization of maxwell’s demon. *Nature*. **561**, 83–87 (2018).
- [49] C. Monroe, W. C. Campbell, L.-M. Duan, Z.-X. Gong, A. V. Gorshkov, P. W. Hess, R. Islam, K. Kim, N. M. Linke, G. Pagano, P. Richerme, C. Senko, and N. Y. Yao, Programmable quantum simulations of spin systems with trapped ions, *Rev. Mod. Phys.* **93**, 025001 (2021).
- [50] C. Monroe and J. Kim, Scaling the ion trap quantum processor, *Science* **339**, 1164 (2013).
- [51] K. Wright, K. M. Beck, S. Debnath, J. M. Amini, Y. Nam, N. Grzesiak, J.-S. Chen, N. C. Pisenti, M. Chmielewski, C. Collins, K. M. Hudek, J. Mizrahi, J. D. Wong-Campos, S. Allen, J. Apisdorf, P. Solomon, M. Williams, A. M. Ducore, A. Blinov, S. M. Kreike-meier, V. Chaplin, M. Keesan, C. Monroe, and J. Kim, Benchmarking an 11-qubit quantum computer, *Nature Communications* **10** (2019), 10.1038/s41467-019-13534-2.
- [52] I. Pogorelov, T. Feldker, C. D. Marciniak, L. Postler, G. Jacob, O. Kriegelsteiner, V. Podlesnic, M. Meth, V. Negnevitsky, M. Stadler, B. Höfer, C. Wächter, K. Lakhmanskii, R. Blatt, P. Schindler, and T. Monz, Compact ion-trap quantum computing demonstrator, *PRX Quantum* **2**, 020343 (2021).
- [53] J. M. Pino, J. M. Dreiling, C. Figgatt, J. P. Gaebler, S. A. Moses, M. S. Allman, C. H. Baldwin, M. Foss-Feig, D. Hayes, K. Mayer, C. Ryan-Anderson, and B. Neyenhuis, Demonstration of the trapped-ion quantum ccd computer architecture, *Nature* **592**, 209–213 (2021).
- [54] L. Egan., D. M. Debroy., C. Noel., A. Risinger., D. Zhu., D. B. ., M. N. ., M. L. ., K. R. Brown., M. Cetina., and C. Monroe, Quantum supremacy using a programmable superconducting processor. *Nature*. **598**, 281–286 (2021).
- [55] M. H. Devoret and R. J. Schoelkopf, Superconducting circuits for quantum information: An outlook, *Science* **339**, 1169 (2013).
- [56] S. Cao, B. Wu, and F. C. et al, Generation of genuine entanglement up to 51 superconducting qubits. *Nature*. **619**, 738 (2023).
- [57] F. Arute, K. Arya, and R. B. et al, Quantum supremacy using a programmable superconducting processor. *Nature*. **574**, 505 (2019).

- [58] W. Yulin, B. Wan-Su, S. Cao, and C. F. et al, Strong quantum computational advantage using a superconducting quantum processor, *Phys. Rev. Lett.* **127**, 180501 (2021).
- [59] Q. Zhu, S. Cao, and F. C. et al, Quantum computational advantage via 60-qubit 24-cycle random circuit sampling, *Science Bulletin* **67**, 240 (2022).
- [60] R. R. Puri, *Mathematical Methods of Quantum Optics*, 1st ed., Springer Series in Optical Sciences, Vol. 79 (Springer Berlin, Heidelberg, 2001).
- [61] K. Wodkiewicz and J. H. Eberly, Coherent states, squeezed fluctuations, and the $su(2)$ and $su(1,1)$ groups in quantum-optics applications, *J. Opt. Soc. Am. B* **2**, 458 (1985).
- [62] B. Yurke, S. L. McCall, and J. R. Klauder, $Su(2)$ and $su(1,1)$ interferometers, *Phys. Rev. A* **33**, 4033 (1986).
- [63] P. K. Aravind, Pseudospin approach to the dynamics and squeezing of $su(2)$ and $su(1, 1)$ coherent states, *J. Opt. Soc. Am. B* **5**, 1545 (1988).
- [64] R. Y. Chiao and T. F. Jordan, Lorentz-group berry phases in squeezed light, *Physics Letters A* **132**, 77 (1988).
- [65] R. M. y Romero, H. Núñez-Yépez, and A. Salas-Brito, An algebraic $su(1,1)$ solution for the relativistic hydrogen atom, *Physics Letters A* **339**, 259 (2005).
- [66] F. Werner and Y. Castin, Unitary gas in an isotropic harmonic trap: Symmetry properties and applications, *Phys. Rev. A* **74**, 053604 (2006).
- [67] S. Deng, Z.-Y. Shi, P. Diao, Q. Yu, H. Zhai, R. Qi, and H. Wu, Observation of the efimovian expansion in scale-invariant fermi gases, *Science* **353**, 371 (2016).
- [68] C. Lv, R. Zhang, and Q. Zhou, $su(1,1)$ echoes for breathers in quantum gases, *Phys. Rev. Lett.* **125**, 253002 (2020).
- [69] J. Zhang, X. Yang, C. Lv, S. Ma, and R. Zhang, Quantum dynamics of cold atomic gas with $su(1,1)$ symmetry, *Phys. Rev. A* **106**, 013314 (2022).
- [70] M. BANDER and C. ITZYKSON, Group theory and the hydrogen atom (i), *Rev. Mod. Phys.* **38**, 330 (1966).
- [71] C. C. Gerry, Berry's phase in the degenerate parametric amplifier, *Phys. Rev. A* **39**, 3204 (1989).
- [72] D. T. Son, Vanishing bulk viscosities and conformal invariance of the unitary fermi gas, *Phys. Rev. Lett.* **98**, 020604 (2007).
- [73] E. Elliott, J. A. Joseph, and J. E. Thomas, Observation of conformal symmetry breaking and scale invariance in expanding fermi gases, *Phys. Rev. Lett.* **112**, 040405 (2014).
- [74] C. Lyu, C. Lv, and Q. Zhou, Geometrizing quantum dynamics of a bose-einstein condensate, *Phys. Rev. Lett.* **125**, 253401 (2020).
- [75] Y.-Y. Chen, P. Zhang, W. Zheng, Z. Wu, and H. Zhai, Many-body echo, *Phys. Rev. A* **102**, 011301 (2020).
- [76] Y. Cheng and Z.-Y. Shi, Many-body dynamics with time-dependent interaction, *Physical Review A* **104** (2021), 10.1103/physreva.104.023307.
- [77] X. Chen, A. Ruschhaupt, S. Schmidt, A. del Campo, D. Guéry-Odelin, and J. G. Muga, Fast optimal frictionless atom cooling in harmonic traps: Shortcut to adiabaticity, *Phys. Rev. Lett.* **104**, 063002 (2010).
- [78] D. Guéry-Odelin, A. Ruschhaupt, A. Kiely, E. Torrontegui, S. Martínez-Garaot, and J. G. Muga, Shortcuts to adiabaticity: Concepts, methods, and applications, *Rev. Mod. Phys.* **91**, 045001 (2019).
- [79] M. Demirplak and S. A. Rice, Adiabatic population transfer with control fields, *J. Phys. Chem. A* **107**, 9937 (2003).
- [80] M. V. Berry, Transitionless quantum driving, *J. Phys. A: Math. Theor.* **42**, 365303 (2009).
- [81] W. Liu, Y. Ke, and C. Lee, Shortcuts to adiabatic thoughtless pumping, (2024), arXiv:2401.17081 [quant-ph].
- [82] J. D. Matrasulov, J. R. Yusupov, and K. S. Matyokubov, Fast forward problem for adiabatic quantum dynamics: Estimation of the energy cost, (2024), arXiv:2407.15250 [quant-ph].